Thermal emission and design in 2D-periodic metallic photonic crystal slabs

David L. C. Chan, Marin Soljačić and J. D. Joannopoulos

Department of Physics and Center for Materials Science and Engineering, Massachusetts Institute of Technology, Cambridge, Massachusetts 02139

dlcchan@mit.edu

Abstract: We present a useful framework within which we can understand some of the physical phenomena that drive thermal emission in 2D-periodic metallic photonic crystal slabs, emphasizing phenomenology and physical intuition. Through detailed numerical calculations for these systems, we find that periodicity plays a key role in determining the types of physical phenomena that can be excited. We identify two structures as good candidates for thermal design, and conclude with a discussion of how the emissive properties of these systems can be tailored to our needs.

OCIS codes: (000.6800) Theoretical physics; (160.4670) Optical properties; (350.5610) Radiation.

References and links

1. M. Planck, "On the Law of Distribution of Energy in the Normal Spectrum," Annalen der Physik **4**, 553–563 (1901).
2. M. Scalora, M. J. Bloemer, A. S. Pethel, J. P. Dowling, C. M. Bowden, and A. S. Manka, "Transparent, metallo-dielectric, one-dimensional, photonic band-gap structures," J. Appl. Phys. **83**, 2377–2383 (1998).
3. S. Y. Lin, J. G. Fleming, D. L. Hetherington, B. K. Smith, R. Biswas, K. M. Ho, M. M. Sigalas, W. Zubrzycki, S. R. Kurtz, and J. Bur, "A three-dimensional photonic crystal operating at infrared wavelengths," Nature **394**, 251–253 (1998).
4. C. M. Cornelius and J. P. Dowling, "Modification of Planck blackbody radiation by photonic band-gap structures," Phys. Rev. A **59**, 4736–4746 (1999).
5. M. Boroditsky, R. Vrijen, T. F. Krauss, R. Coccioli, R. Bhat, and E. Yablonovitch, "Spontaneous Emission Extraction and Purcell Enhancement from Thin-Film 2-D Photonic Crystals," J. Lightwave Technol. **17**, 2096–(1999).
6. S.-Y. Lin, J. G. Fleming, E. Chow, J. Bur, K. K. Choi, and A. Goldberg, "Enhancement and suppression of thermal emission by a three-dimensional photonic crystal," Phys. Rev. B **62**, R2243–R2246 (2000).
7. A. A. Erchak, D. J. Ripin, S. Fan, P. Rakich, J. D. Joannopoulos, E. P. Ippen, G. S. Petrich, and L. A. Kolodziejski, "Enhanced coupling to vertical radiation using a two-dimensional photonic crystal in a semiconductor light-emitting diode," Appl. Phys. Lett. **78**, 563–565 (2001).
8. H. Sai, H. Yugami, Y. Akiyama, Y. Kanamori, and K. Hane, "Spectral control of thermal emission by periodic microstructured surfaces in the near-infrared region," J. Opt. Soc. Am. A **18**, 1471–1476 (2001).
9. J.-J. Greffet, R. Carminati, K. Joulain, J.-P. Mulet, S. Mainguy, and Y. Chen, "Coherent emission of light by thermal sources," Nature **416**, 61–64 (2002).
10. J. G. Fleming, S. Y. Lin, I. El-Kady, R. Biswas, and K. M. Ho, "All-metallic three-dimensional photonic crystals with a large infrared bandgap," Nature **417**, 52–55 (2002).
11. S. Y. Lin, J. Moreno, and J. G. Fleming, "Three-dimensional photonic-crystal emitter for thermal photovoltaic power generation," Appl. Phys. Lett. **83**, 380–382 (2003).
12. S.-Y. Lin, J. Moreno, and J. G. Fleming, "Response to Comment on 'Three-dimensional photonic-crystal emitter for thermal photovoltaic power generation'," Appl. Phys. Lett. **84**, 1999 (2004).
13. H. Sai, T. Kamikawa, Y. Kanamori, K. Hane, H. Yugami, and M. Yamaguchi, "Thermophotovoltaic Generation with Microstructured Tungsten Selective Emitters," in *Proceedings of the Sixth NREL Conference on Thermophotovoltaic Generation of Electricity*, pp. 206–214 (2004).

#70215 - $15.00 USD Received 24 April 2006; revised 13 August 2006; accepted 27 August 2006

14. A. Narayanaswamy and G. Chen, "Thermal emission control with one-dimensional metallodielectric photonic crystals," Phys. Rev. B **70**, 125101–125104 (2004).
15. C. Luo, A. Narayanaswamy, G. Chen, and J. D. Joannopoulos, "Thermal Radiation from Photonic Crystals: A Direct Calculation," Phys. Rev. Lett. **93**, 213905–213908 (2004).
16. B. J. Lee, C. J. Fu, and Z. M. Zhang, "Coherent thermal emission from one-dimensional photonic crystals," Appl. Phys. Lett. **87**, 071904–071906 (2005).
17. I. Celanovic, D. Perreault, and J. Kassakian, "Resonant-cavity enhanced thermal emission," Phys. Rev. B **72**, 075127–075132 (2005).
18. M. Florescu, H. Lee, A. J. Stimpson, and J. Dowling, "Thermal emission and absorption of radiation in finite inverted-opal photonic crystals," Phys. Rev. A **72**, 033821–033829 (2005).
19. A. Mekis, A. Dodabalapur, R. E. Slusher, and J. D. Joannopoulos, "Two-dimensional photonic crystal couplers for unidirectional light output," Opt. Lett. **25**, 942–944 (2000).
20. M. U. Pralle, N. Moelders, M. P. McNeal, I. Puscasu, A. C. Greenwald, J. T. Daly, E. A. Johnson, T. George, D. S. Choi, I. El-Kady, and R. Biswas, "Photonic crystal enhanced narrow-band infrared emitters," Appl. Phys. Lett. **81**, 4685–4687 (2002).
21. S. Enoch, J.-J. Simon, L. Escoubas, Z. Elalmy, F. Lemarquis, P. Torchio, and G. Albrand, "Simple layer-by-layer photonic crystal for the control of thermal emission," Appl. Phys. Lett. **86**, 261101–261103 (2005).
22. M. Laroche, R. Carminati, and J.-J. Greffet, "Coherent Thermal Antenna Using a Photonic Crystal Slab," Phys. Rev. Lett. **96**, 123903–123906 (2006).
23. S. Fan and J. D. Joannopoulos, "Analysis of guided resonances in photonic crystal slabs," Phys. Rev. B **65**, 235112–235119 (2002).
24. S. Peng and G. M. Morris, "Resonant scattering from two-dimensional gratings," J. Opt. Soc. Am. A **13**, 993–(1996).
25. A. R. Cowan, P. Paddon, V. Pacradouni, and J. F. Young, "Resonant scattering and mode coupling in two-dimensional textured planar waveguides," J. Opt. Soc. Am. A **18**, 1160–1170 (2001).
26. M. Meier, A. Mekis, A. Dodabalapur, A. Timko, R. E. Slusher, and J. D. Joannopoulos, "Laser action from two-dimensional distributed feedback in photonic crystals," Appl. Phys. Lett. **74**, 7–9 (1999).
27. A. Taflove and S. C. Hagness, *Computational Electrodynamics: The Finite-Difference Time-Domain Method* (Artech House, Norwood, MA, 2000).
28. M. A. Ordal, R. J. Bell, J. R. W. Alexander, L. L. Long, and M. R. Querry, "Optical properties of fourteen metals in the infrared and far infrared: Al, Co, Cu, Au, Fe, Pb, Mo, Ni, Pd, Pt, Ag, Ti, V and W," Appl. Opt. **24**, 4493–(1985).

1. Introduction

A blackbody is defined as an object of perfect absorption. Its entropy is maximized, and in that sense it exemplifies utter disorder. The physics of blackbodies has both fascinated and intrigued scientists for well over a century now [1]. In practice, most objects have only finite absorption, and are thus referred to as 'graybodies'. However, graybodies are of interest because their thermal emission spectra can be changed by altering the geometry of the system or the materials used. The ability to modify or tailor the thermal emission profile of an object is of great importance and interest in many areas of applied physics and engineering. It has been noted that periodic sub-wavelength scale patterning of metallo-dielectric systems, i.e. photonic crystals, can modify their emission spectra in interesting ways [2, 3, 4, 5, 6, 7, 8, 9, 10, 11, 12, 13, 14, 15, 16, 17, 18]. Thermal radiation from 2D-periodic photonic crystals has been studied within the contexts of spectral and directional control [19, 8, 20, 21, 22], guided resonances [23], thermophotovoltaic generation [13], resonant scattering [24, 25], laser action [26], Kirchhoff's law [15], coherence [9, 22], and spontaneous emission enhancement [5, 7, 20].

In this article, we focus on some of the most important physical phenomena that give rise to many of the features observed in thermal emission spectra of 2D-periodic metallic photonic crystal slabs, with the intention of developing physical intuition and understanding of features of emission spectra. We demonstrate through detailed numerical studies the key role played by periodicity in determining the types of physical phenomena that can be thermally excited in 2D-periodic metallic photonic crystals. We develop understanding and physical insight using two illustrative examples, before applying them to hybrid structures. Such structures exhibit strong

#70215 - $15.00 USD Received 24 April 2006; revised 13 August 2006; accepted 27 August 2006

thermal emission peaks which can be used as building blocks in thermal design. We show how one can tailor the emissive properties of these structures to one's design needs by changing two simple physical parameters.

2. Description of numerical methods

Kirchhoff's law states that for an object in thermal equilibrium with the surrounding radiation field, its absorptivity and emissivity are equal, for every frequency, direction, and polarization. Thus, to study thermal emission of an object, we need simply calculate its absorptivity spectrum, knowing that the object's absorptivity and emissivity spectra are identical. Moreover, for the purposes of developing an intuitive understanding of the physics behind thermal emission, it is often more helpful to think in terms of absorption rather than emission, and it is on this basis that we will proceed.

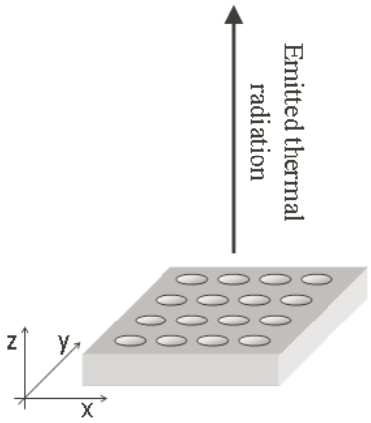

Fig. 1. Schematic illustrating the geometry of a typical system. The *x*- and *y*-axes are defined in the plane of the slab, with the *z*-direction coming out of the slab. We study the thermal radiation being emitted in the perpendicular direction.

Figure 1 is a schematic illustrating the geometry of a typical system under investigation. It is important to note that because of the mirror symmetry of the system in a plane perpendicular to *x* and *y*, the modes of the system can be separated into transverse electric (TE) and transverse magnetic (TM) modes with respect to the mirror plane. As a result of this symmetry, *x*-polarized modes do not mix with *y*-polarized modes. Thus, we can analyze these two polarizations completely separately, and this is what we do in all our calculations.

Numerical simulations in our work are performed using a finite-difference time-domain (FDTD) algorithm [27]. These are exact (apart from discretization) 3D solutions of Maxwell's equations, including material dispersion and absorption. We choose a computational cell with dimensions $40 \times 40 \times 240$ grid points, corresponding to 40 grid points per lattice constant a. The faces of the cell normal to the *x* and *y* axes are chosen to have periodic boundary conditions, while the faces normal to the *z*-axis (i.e. the top and bottom ones) have perfectly matched layers (PML) to prevent reflection. In other words, this is a 3D simulation of a 2D-periodic system. The PhC slab is in the middle, and flux planes are placed on either side of it at least $2a$ away. We run the simulation for a total of 40,000 time steps, chosen to be sufficiently large to allow resolution of peaks with quality factors (Q) up to 250. We illuminate the photonic crystal slab with a normally incident, temporally Gaussian pulse. We record the fields going through flux planes on either side of the slab and perform a discrete Fourier-transform on the time-series of fields, which

#70215 - $15.00 USD Received 24 April 2006; revised 13 August 2006; accepted 27 August 2006

we use to calculate fluxes as functions of frequency, $\Phi(\omega) = \frac{1}{2}\mathrm{Re}\{\int \mathbf{E}^*(\mathbf{r},\omega) \times \mathbf{H}(\mathbf{r},\omega) \cdot \mathrm{d}\mathbf{S}\}$. We run the simulation once with the slab in place, and again with vacuum only, such that $\mathbf{E}_{slab} = \mathbf{E}_{vac} + \mathbf{E}_{ref}$, with $\mathbf{E}_{ref}$ being the field due to reflection. The reflectance is given by

$$R(\omega) \equiv \frac{\Phi_{ref}}{\Phi_{vac}} = \frac{-\frac{1}{2}\mathrm{Re}\{\int_{A_1}[\mathbf{E}_{slab}(\mathbf{r},\omega) - \mathbf{E}_{vac}(\mathbf{r},\omega)]^* \times [\mathbf{H}_{slab}(\mathbf{r},\omega) - \mathbf{H}_{vac}(\mathbf{r},\omega)] \cdot \mathrm{d}\mathbf{S}\}}{\frac{1}{2}\mathrm{Re}\{\int_{A_1} \mathbf{E}^*_{vac}(\mathbf{r},\omega) \times \mathbf{H}_{vac}(\mathbf{r},\omega) \cdot \mathrm{d}\mathbf{S}\}} \quad (1)$$

where A_1 is the flux plane corresponding to '1', and the minus sign in the numerator is there to make the reflected flux positive. This expression can be shown to simplify to $R(\omega) = [\Phi_1^{vac}(\omega) - \Phi_1^{slab}(\omega)]/\Phi_1^{vac}(\omega)$ where the flux plane closer to the light source is '1', and the flux plane further from the light source is '2'. (One can show that the numerator becomes $\Phi_1^{vac}(\omega) - \Phi_1^{slab}(\omega) + \frac{1}{2}\mathrm{Re}\{\int_{A_1}(\mathbf{E}^*_{vac} \times \mathbf{H}_{ref} - \mathbf{H}_{vac} \times \mathbf{E}^*_{ref}) \cdot \mathrm{d}\mathbf{S}\}$ but the cross term vanishes for incoming and outgoing plane waves in vacuum, for which **E** and **H** are proportional.) Similarly, the transmittance is given by $T(\omega) = \Phi_2^{slab}(\omega)/\Phi_2^{vac}(\omega)$ and the absorbance is simply $A(\omega) = 1 - R(\omega) - T(\omega)$. This way, we obtain reflectance, transmittance and absorbance spectra for PhC slabs. We incorporate absorption into our simulations by means of the Drude model, according to the following equation:

$$\varepsilon(\omega) = \varepsilon_\infty + \frac{\sigma}{(\omega_0^2 - \omega^2 - i\gamma\omega)} \quad (2)$$

where ε_∞, γ, ω_0 and σ are input parameters. In our case, we are concerned with metals, for which $\omega_0 = 0$. By Kirchhoff's law, the absorbance spectra so calculated are identical to the emittance spectra of these objects, for each polarization, frequency and observation angle.

3. Holes and dips

Let us now turn our attention to real systems and the physical effects that are manifested therein. The goal is to develop an understanding of the physical processes that drive emittance in these systems. The first structure we will examine is a simple metal slab with holes (see Fig. 2). If we illuminate the structure with light incident from the top of the cell, the light propagates down the holes which act as metallic waveguides. Waveguide cut-offs arise from the requirement that the parallel component of the electric field be continuous across a boundary. Inside a perfect metal, the electric field is strictly zero. For such a material, $E_\parallel$ is constrained to vanish at the surface, and this leads to the well-known cut-off frequency corresponding to a half-wavelength oscillation. Below this frequency, no propagating mode can be supported within the waveguide, because the boundary condition cannot be satisfied. For a realistic metal (i.e. one that permits some penetration of fields), the fields are not required to exactly vanish at the surface, but must decay away rapidly and exponentially once inside the material. Such boundary condition matching leads to a similar cut-off as in the case of the perfect metal, except that the penetration of field into the metal produces a cut-off with a slightly lower frequency, because the *effective* width of the waveguide is slightly larger. Cut-off frequencies depend on the width of the waveguide. The wider the waveguide, the lower the cut-off frequency.

We present emittance and transmittance spectra for this system. Figure 2(a) shows how the spectra change with hole radius. The peaks below 1.0 (indicated by black arrows) are waveguide cut-offs arising from propagation of light through the holes. These peaks decrease in frequency with increasing radius, a clear signature of waveguide cut-offs. They correspond to modes that fit approximately half a wavelength across the hole in the *x*-direction. As we discussed, the electric field has to be continuous as we cross media boundaries in the *x*-direction (because E_y is parallel to the media boundary) but not in the *y*-direction. Thus, these modes have one 'hump' as we cross the holes in the *x*-direction, and decay exponentially inside the metallic bulk between

#70215 - $15.00 USD Received 24 April 2006; revised 13 August 2006; accepted 27 August 2006

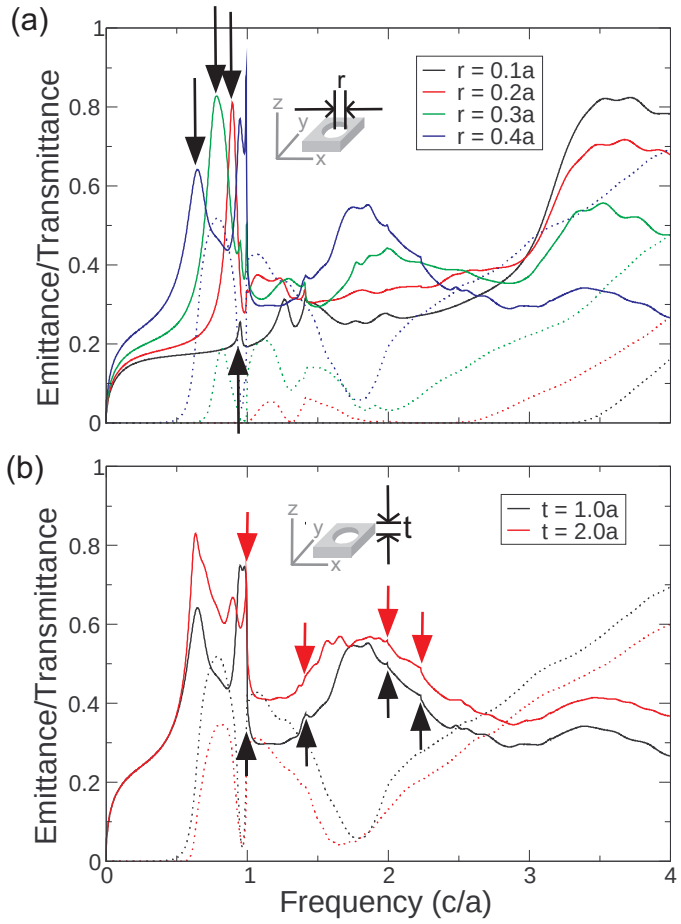

Fig. 2. (Color) Here we show emittance (solid lines) and transmittance (dotted lines) spectra for a 2D-periodic metal slab with circular holes, viewed at normal incidence and for *y*-polarized light. The Drude parameters used for the metal are $\varepsilon_\infty = 1$, $\omega_0 = 0$, $\gamma = 0.3(2\pi c/a)$ and $\omega_p = \sqrt{10}(2\pi c/a)$. In Panel (a), we fix the thickness of the slab at $1.0a$ (where a is the lattice constant of the slab) and vary the radius of the holes. The black arrows indicate the peaks produced by the waveguide cut-off in the *x*-direction. In Panel (b), we keep the hole radius constant at $0.4a$ and vary the thickness of the slab. Here, we use arrows to indicate the peaks produced by diffraction.

#70215 - $15.00 USD Received 24 April 2006; revised 13 August 2006; accepted 27 August 2006

holes such that the field profile within the metal is of the form of a hyperbolic sine/cosine curve (a combination of a decaying and growing exponential), depending on parity. We can see immediately that as we increase the radius of such a hole, the profile relaxes in the *x*-direction in such a way as to make the hump wider. This leads to a larger effective *x*-wavelength for the mode, and thus a lower frequency cut-off. (The wavelength in the *y*-direction is unaffected by the radius of the hole, since E_y is not required to be continuous in the *y*-direction.)

Diffraction peaks occur when we consider the slab system at a macroscopic level, in terms of incoming and outgoing radiation modes. This effect is not unique to metallic PhCs, and can be observed in non-metallic PhCs as well. In terms of absorption, the incident light, being normal, can couple into outgoing radiation modes (in transmission or reflection) that conserve the wave vector up to a reciprocal lattice vector in a direction of discrete periodicity. Because the incident light has no $k_{transverse}$ component, it can couple into outgoing modes with $k_{transverse}$ equal to an integer multiple of $2\pi/a$ (i.e. 1 in our units). This means that as we increase the frequency of the incoming radiation, a new diffraction direction will be coupled into at $\omega = 1, \sqrt{2}, 2, \sqrt{5}...$, corresponding to $(k_x, k_y) = (1,0), (1,1), (2,0), (2,1)...$ At the threshold frequency for a new diffraction mode, the wave vector has no k_z component, and so $\mathbf{k}$ is parallel to the surface of the slab. Such 'grazing' modes have maximum interaction with the slab because they travel close to the surface of the metal, and as such are strongly absorbed by the material. These absorption peaks translate into emission peaks, via Kirchhoff's law, so we would expect to see emission peaks for modes corresponding to $\omega = |k| = 1, \sqrt{2}, 2, \sqrt{5}...$

Figure 2(b) shows how emittance and transmittance change with the thickness of the metal slab. First, we notice that transmittance is greater for the thinner slab, as one would expect. Second, we see the emergence of diffraction peaks at $1, \sqrt{2}, 2$ and $\sqrt{5}$ (we indicate these with red and black arrows). Not only do they occur at precisely those frequencies that correspond to the root of the sum of two squares (their wave vectors being permutations of (1, 0), (1, 1), (2, 0) and (2, 1), respectively), they are also the same for both black and red curves, lending further weight to the argument that they are diffraction peaks. Their magnitudes are clearly quite variable; indeed, they wash out at higher frequencies. Such diffraction peaks can be seen in Fig. 2(a), too.

What happens if we take the same metal slab, but do not drill holes in the slab that go all the way through? What happens if, instead of having circular holes, we have circular *dips*? We present emittance and transmittance for this structure in Fig. 3 as a function of dip radius. Again, we see peaks below 1.0 which correspond to cut-offs, except in this case they are not waveguide cut-offs but a kind of 'cavity' cut-off, where k_x is such that there is approximately half a wavelength in the *x*-direction. We see diffraction peaks at $1, \sqrt{2}, 2$ and $\sqrt{5}$. Above $\omega_p = \sqrt{10} \approx 3.16$, the plasmon frequency of the metal, transmittance becomes significant, because above that frequency, the metal becomes transparent and light can pass through it as though it were a dielectric material (while still being subject to some absorptive loss).

4. Hybrid structures

Let us now turn our attention to hybrid structures which involve both metal and dielectric. We consider a metal slab with a circular dielectric puck on top. This puck is intended to be a small perturbation to the system that introduces discrete periodicity in both the *x*- and *y*-directions by means of a piece of dielectric. We observe emitted light at normal incidence and polarized in the *y*-direction.

Figure 4(a) shows how emittance and transmittance vary with the dielectric constant of the perturbation (ε). First, we observe many peaks in the emittance spectra, and we note that the positions of some these peaks (particularly the ones at frequencies less than 2.0) decrease with increasing ε. Second, we see zero transmittance in the system for frequencies below $\omega_p \approx$

#70215 - $15.00 USD Received 24 April 2006; revised 13 August 2006; accepted 27 August 2006

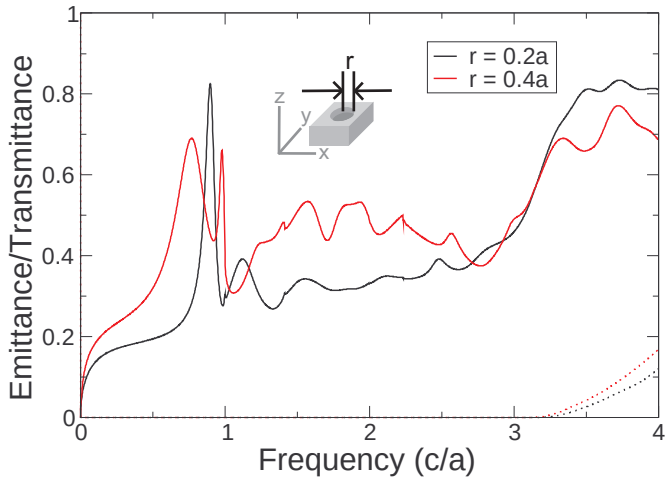

Fig. 3. (Color) We show emittance (solid lines) and transmittance (dotted lines) spectra for a 2D-periodic metal slab of thickness $1.0a$ with circular dips, observed at normal incidence and y-polarization. The dips have a depth of $0.5a$. The Drude parameters used are $\varepsilon_\infty = 1$, $\omega_0 = 0$, $\gamma = 0.3(2\pi c/a)$ and $\omega_p = \sqrt{10}(2\pi c/a)$. We show spectra for two different radii of dips, keeping the slab thickness constant.

3.16, as we expect, because the metal is opaque at frequencies below the plasmon frequency. Third, we see also an entire series of diffraction peaks, at frequencies 1, $\sqrt{2}$, 2, $\sqrt{5}$, $2\sqrt{2}$ and 3, corresponding to modes with wave vectors (1, 0), (1, 1), (2, 0), (2, 1) and permutations thereof. These are especially clearly seen on the black curve. We know they are diffraction peaks because they not only fit the above sequence, but also have the same frequencies on the red and green curves. (Diffraction peaks do not change with the dielectric constants of the structure.) Fourth, we demonstrate that most of the emittance peaks with frequencies below 2.0 that we see in Fig. 4(a) are in fact produced by surface plasmons.

Surface plasmons (SPs) are excitations that exist on the interface between a plane-metal and a dielectric. They are confined to the surface, but can propagate freely within that surface. They have a relatively simple dispersion relation that is approximately linear at low wave vectors and bends over toward a flat cut-off at higher wave vectors ($\omega_p/\sqrt{\varepsilon+1}$ is the cut-off frequency, where ω_p is the plasmon frequency and ε is the dielectric constant). If the direction of propagation is x (i.e. $\mathbf{k}$ is in the x-direction), then the SP will have field components E_x, E_z and H_y (the z-direction is normal to the interface). The SP is unusual in that it has an electric field component in the direction of propagation. Normally incident light (for which $k_{transverse} = 0$) cannot couple into SP modes with non-zero k because of conservation of wave vector; however, it *can* couple into such modes if the wave vector of the SP is along a direction of discrete translational symmetry, because in such a direction, wave vector is conserved only up to an integer multiple of the reciprocal lattice vector. These correspond to $\mathbf{k} = (m,n)(2\pi/a)$ where m and n are integers.

To show that the emittance peaks with frequencies below 2.0 are indeed SPs, we record the frequencies of the peaks (up to $\omega_p/\sqrt{\varepsilon+1}$, the SP cut-off) for each curve in Fig. 4(a), and

#70215 - $15.00 USD Received 24 April 2006; revised 13 August 2006; accepted 27 August 2006

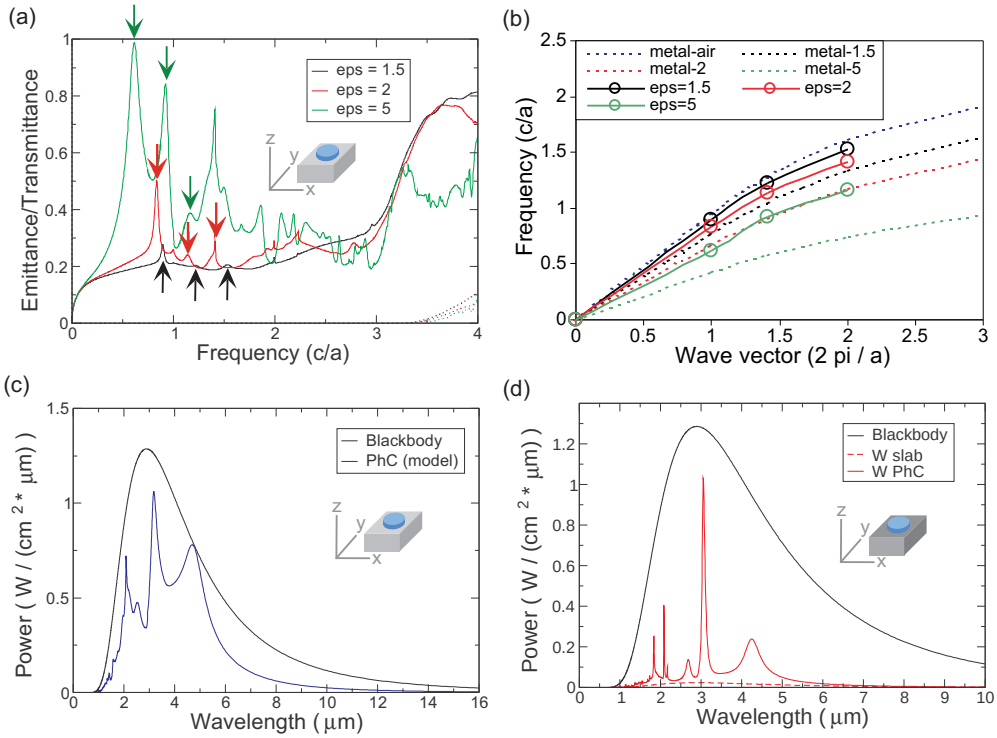

Fig. 4. (Color) Panel (a) shows emittance (solid lines) and transmittance (dotted lines) spectra for a 2D-periodic metal slab of thickness $1.0a$ with circular dielectric pucks for normal incidence and light polarized in the y-direction. The pucks have a radius of $0.4a$ and a thickness of $0.2a$. The Drude parameters used for the metal are $\varepsilon_\infty = 1$, $\omega_0 = 0$, $\gamma = 0.3(2\pi c/a)$ and $\omega_p = \sqrt{10}(2\pi c/a)$. We show spectra for three different dielectric constants for the circular puck. In Panel (b), we took the peaks labeled by arrows in Panel (a), and plotted them on a dispersion curve. (Note that the third red peak in Panel (a) coincides with a diffraction peak at frequency $\sqrt{2} \approx 1.41$.) We see that the dispersion of the peaks (lines with circles) lies between the metal-air dispersion and the metal-dielectric dispersion, for the corresponding dielectric constant. Therefore, it is quite plausible that these peaks are produced by surface plasmon modes. In Panel (c), we show the thermal emission spectrum for the same metal slab with pucks of dielectric constant $\varepsilon = 5$ at temperature 1000K (we call it "PhC (model)"). We also show the blackbody spectrum at that temperature for comparison. The lattice constant was chosen to be $a = 2.94\mu m$. Panel (d) shows the thermal emission spectrum for the same system except that the "model" metal has been replaced by tungsten. We modeled tungsten with Drude parameters[28] $\varepsilon_\infty = 1$, $\omega_0 = 0$, $\gamma/(2\pi c) = 487cm^{-1}$ and $\omega_p/(2\pi c) = 51700cm^{-1}$, and we chose $a = 2.94\mu m$. We show the emission spectra for a uniform tungsten slab of thickness a (without pucks) and a blackbody for comparison.

#70215 - $15.00 USD
Received 24 April 2006; revised 13 August 2006; accepted 27 August 2006

plot them as circles in Fig. 4(b) against wave vector magnitude, making the assumption that the first peak has a wave vector of (0, 1), the second a wave vector of (1, 1), and the third a wave vector of (0, 2) (all in units of $2\pi/a$). We make this assumption because this sequence of $(k_x, k_y) = (m, n)$ produces a sequence of frequencies in ascending order. In addition, we plot SP dispersion curves for metal-air and metal-dielectric structures where both media are semi-infinite in extent (dotted lines). SP modes in the structure under consideration would therefore be expected to have a dispersion relation that lies between the metal-air and the metal-dielectric dispersions, since the average dielectric constant of the dielectric strip/air lies between that of the air and the dielectric. Thus, we would expect the black circles to lie between the dotted black and blue curves, the red circles to lie between the dotted red and blue curves, and so on. Indeed, this is exactly what we see. Furthermore, the fact that the circles, when joined together by solid lines, form a dispersion relation that clearly bends over toward a cut-off, gives us confidence in identifying these modes as SPs.

We can obtain the emissive power of these structures by taking the emittance spectra that we have calculated and multiplying them by the blackbody emission spectrum (which is also known as the Planck distribution). This is what we did in Fig. 4(c). We chose $a = 2.94\mu m$ and plotted thermal emission of the PhC slab as a function of wavelength. We show the emission spectrum of a blackbody for comparison. We can immediately see an emission peak near $4.7\mu m$ that has as high emission as a blackbody; this peak corresponds to the first SP peak in Fig. 4(a). The two emission peaks at approximately $2.1\mu m$ and $3.2\mu m$ are diffraction and SP peaks, respectively.

In Fig. 4(d), we consider the same structure except that the "model" metal slab is now replaced by a tungsten slab. We did this by doing the calculation using the Drude parameters of tungsten. We also plot the equivalent tungsten slab emittance (dashed red curve) for comparison. In keeping with Kirchhoff's law, at no point does the emission of the PhC structure exceed that of a blackbody. The qualitative similarities between this emission spectrum and that shown in Fig. 4(c) can be traced quite easily: the three major peaks remain; the tall central peak and the peak to its right are SPs, while the sharp peak to the left (around $2\mu m$) comes from diffraction into (1, 1) modes. Overall, the background emission of the tungsten PhC slab is lower than that for the "model" metal that we have hitherto been studying, because the background emittance of a slab[15] goes as $2\gamma/\omega_p$ (in regime $\gamma < \omega < \omega_p$), and ω_p is much higher for tungsten than for the Drude metal in Fig. 4(c). Notice that the PhC tungsten slab has higher emission at *all* frequencies than the uniform tungsten slab. Thus, we have excellent enhancement of emissive power through the use of a PhC.

As we have already remarked, the dominant feature of the emission characteristics of this structure is the central peak at $3.06\mu m$, which achieves 80% of the emission of a blackbody. As we will show in Fig. 5, it is possible to shift this peak by changing the lattice constant of the structure. By so doing, we can place a strong emission peak at whatever frequency we choose. If we combine copies of this structure with different lattice constants, we can place strong emission peaks at multiple frequencies. This is the beginning of thermal design using 2D-periodic metallic PhC slabs.

5. Thermal design

In order to facilitate our discussion of thermal design in 2D-periodic metallic photonic crystals, we turn our attention to another variation on the theme of a hybrid structure, and show how the emission spectrum of this structure can be tailored to our needs. We study a tungsten slab on top of which sits a dielectric slab with circular holes. One can think of the dielectric portion of this structure as being the 'inverse' of the circular puck. Such a structure exhibits discrete periodicity in both the *x*- and *y*-directions.

#70215 - $15.00 USD Received 24 April 2006; revised 13 August 2006; accepted 27 August 2006

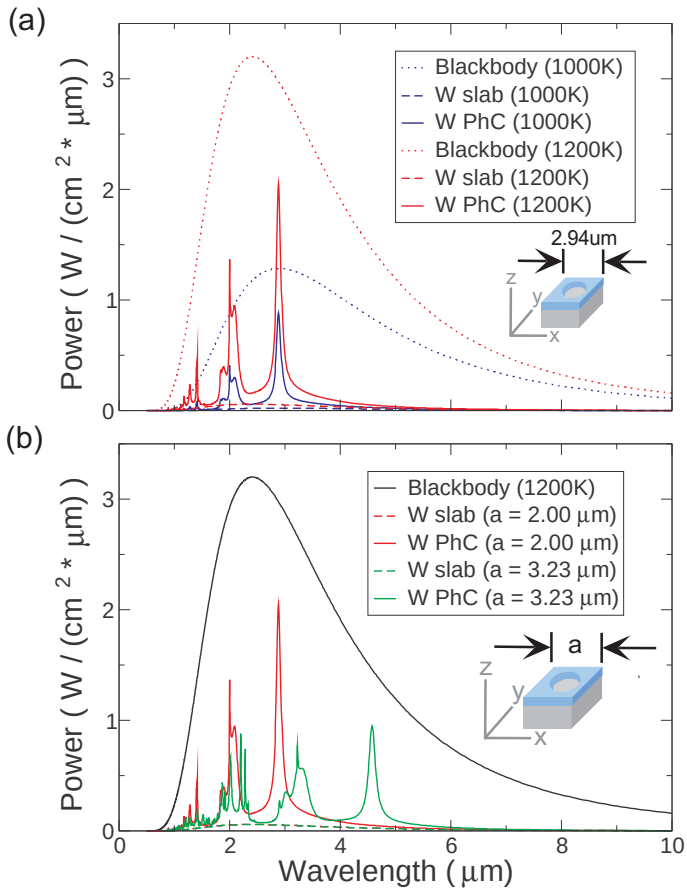

Fig. 5. (Color) Here we show the thermal emission spectrum for a hybrid 2D-periodic structure consisting of a tungsten slab and a dielectric slab with holes. The metal slab is $1.0a$ thick while the dielectric slab ($\varepsilon = 5$) is $0.2a$ thick with holes of radius $0.4a$. We show emission of light polarized in the y-direction. In Panel (a), we display emission at two different temperatures. We chose a lattice constant of $a = 2.00\mu m$. In Panel (b), we show how the emissive power changes with lattice constant. In both panels, we show emission spectra for a uniform tungsten slab of thickness a without dielectric, and a blackbody, for comparison.

#70215 - $15.00 USD
Received 24 April 2006; revised 13 August 2006; accepted 27 August 2006

We show the emission spectrum for such a structure in Fig. 5. In Panel (a), we choose $a = 2.00\mu m$ and vary the temperature of operation. We plot thermal emission for the PhC slab, the unadorned tungsten slab, and a blackbody. Again, the PhC emission far exceeds that of a uniform tungsten slab. We see three prominent groups of peaks, the smallest of which has fairly complicated substructure. First, we notice that the positions of the peaks do not change with temperature. Second, increasing temperature increases emission at *all* wavelengths. Emissive power goes as T^4 (Stefan's law), so that, going from 1000K to 1200K, emission increases by a factor of $(1.2)^4 \approx 2.07$ (provided the weighting does not change significantly). Third, the relative weighting given to different wavelengths changes with temperature, because the peak of the Planck distribution shifts toward lower wavelengths with increasing temperature. In our case, the group of small peaks between 1 and $2\mu m$ were insignificant features at 1000K, but became more prominent at 1200K, because the blackbody spectrum shifted in such a way as to give those peaks much more weight than before (thus, they were enhanced by more than a factor of 2.07). Fourth, the emission of the PhC slab exceeds that of the uniform slab at all wavelengths and at all temperatures. In fact, the enhancement is impressive: we see a 20-fold increase in emissive power (over that of a slab) at the major peak at around $2.9\mu m$. Of course, emissivity never exceeds unity, because that would violate the Second Law of Thermodynamics (the large peak in question attains 66% emissivity). The important lesson we learn from this is that we can emphasize different parts of the emission spectrum of a PhC by changing the temperature at which we operate the thermal structure.

In Fig. 5(b), instead of changing the temperature, we keep temperature fixed and vary the lattice constant of the PhC. The blackbody envelope and the emission spectrum of a uniform slab of this same metal are shown for comparison. We see that increasing the lattice constant shifts the emission peaks in the PhC towards a higher wavelength. In our case, for $a = 2.00\mu m$, the large peak is already close to the point of maximum blackbody emission, so that increasing the lattice constant to $a = 3.23\mu m$ only served to decrease the total emission from that excitation (incidentally, it is a surface plasmon). However, the change in a also brought some small peaks from the lower wavelengths into the picture. The point of this exercise is to illustrate the degree of control we have over the position of the peaks, and by these simple techniques, we can shift emissive power around to different parts of the spectrum. It is useful to note that for both choices of a, there is significant enhancement of emission over that of a uniform slab because the breaking of continuous translational symmetry allows more wave vector modes to be excited and coupled into.

The two hybrid structures we considered in this and the previous sections would be suitable candidates for applications that require narrow band emission in one or more frequencies. Both structures have a dominant peak that can be shifted in wavelength by changing the lattice constant. If we want three emission bands separated by 1-$2\mu m$, the structure in Fig. 5 would be a good choice. There are two different ways to amplify an emission peak relative to background emission. We can choose to operate the structure at different temperatures, or we could change the lattice constant. These are simply two different ways of making the emission peak coincide with the wavelength of maximum blackbody emission. By combining many such hybrid structures, each with its own lattice constant, we can place strong emission peaks at whichever wavelengths we choose. We therefore have a means of tailoring the thermal emission properties of a hybrid structure to our needs.

6. Conclusion

We presented a physical and intuitive framework within which we can understand some of the physical phenomena that drive thermal emission in 2D-periodic metallic photonic crystal slabs. We performed detailed numerical calculations for these systems, and found that period-

#70215 - $15.00 USD Received 24 April 2006; revised 13 August 2006; accepted 27 August 2006

icity played a key role in determining the types of physical phenomena that can be excited. In particular, we saw how periodicity gave rise to waveguide cut-offs, waveguide resonances, diffraction peaks and surface plasmon modes. Using hybrid structures composed of metal and dielectric components, we obtained sharp emission enhancement over and above that of a metal slab. In the case of tungsten, we created strong emission peaks with 80% and 66% emissivity, far exceeding that of a uniform tungsten slab, which plateaus at about 3-4%. These peaks could be shifted at will by changing the lattice constant of the structure or by changing the temperature at which the structure is operated. We can design materials with multiple emission peaks by combining hybrid structures, each with its own lattice constant. Thus, we have a powerful set of tools with which to develop physical intuition and understanding for thermal design. The ability to design thermal emission could well find uses in thermophotovoltaic systems and defense applications, where many targeting systems rely on the detection of thermal emission from projectiles.

Acknowledgments

We thank our colleagues Peter Bermel and Steven Johnson at the Massachusetts Institute of Technology for helpful discussions. This work was supported in part by the Croucher Foundation (Hong Kong) and the MRSEC program of the NSF under Grant No. DMR-0213282.

#70215 - $15.00 USD Received 24 April 2006; revised 13 August 2006; accepted 27 August 2006